JPMTR-2407
DOI 10.14622/JPMTR-2407
UDC 519.6:655.3.066:676.2:620.1:658.56

Review paper | 192
Received: 2024-05-27
Accepted: 2024-09-12

Modeling the process of ink transfer from the gravure printing plate to the printing substrate

Svitlana Havenko[1], *Jerzy Czubak*[2], *Yosyf Piskozub*[3], *Yaroslav Uhryn*[2] *and Marta Labetska*[2]

[1]Center of Papermaking and Printing,
Lodz University of Technology,
Str. Wólczańska, 223, Lodz, Poland, 90-924
[2]Printing Art and Media Technologies Institute,
Lviv Polytechnic National University,
Bandera St., 12, Lviv, Ukraine, 79000,
[3]Department of Applied Mathematics,
Faculty of Computer Science and Telecommunications,
Cracow University of Technology,
Warszawska Str. 24, Cracow, Poland, 31-155

svitlana.havenko@p.lodz.pl
jerzyczubak2022@gmail.com
yosyf.piskozub@pk.edu.pl
yaroslav.m.uhryn@lpnu.ua
marta.t.labetska@lpnu.ua

Abstract

The article presents a mathematical model of imprint formation in gravure printing on cardboard substrates. The focus is on ensuring imprint quality by balancing interactions between the structural subsystems of the printing press, specifically the plate cylinder, ink, printing system, and substrate. Using mathematical models, the behavior of the printing substrate and printing plate elements system is investigated by determining the stress–strain state of the contacting elements during imprint formation. The study describes the ink transfer process from the gravure printing plate to the substrate, considering factors such as substrate weight and structure, technical characteristics of the printing press, and its structural subsystems. The method for calculating printing pressure is also examined. At higher printing speeds and pressures, cylinder coatings can be damaged, leading to overheating and cracking, which necessitates cylinder cooling. Increased press width requires greater pressure to achieve the desired contact area, causing cylinder deflection and uneven pressure distribution, affecting image quality and color matching. Morphological analysis confirmed the significant influence of the printing and inking systems of web-fed gravure presses on pressure distribution in the printing zone. The stress–strain state of objects in direct contact is a key factor in imprint quality. Therefore, studying the micromechanics of contacting surfaces during printing is crucial for high-quality images. Mathematical modeling allows calculation and control of the load in the contact zone between the substrate and ink-filled printing elements, ensuring the quality of gravure imprints on various materials.

Keywords: gravure printing, mathematical models, control, print quality

1. Introduction

Despite its high image quality, gravure printing was considered conservative, not very innovative and less profitable compared to flexographic printing a few years ago. This opinion about gravure printing has recently changed thanks to many technological innovations (Anon., 2006). Innovative processes of automation of prepress preparation, as well as the faster process of engraving the printing plates and the shorter preparation time of the gravure printing press, have greatly increased productivity and cost-effectiveness. In Stefanyshena and Zorenko (2020), modern trends in the development of gravure printing are considered based on the analysis of patent sources and scientific and technical literature regarding the technologies of manufacturing printing plates, printing equipment, consumables and areas of application in different geographical regions. Due to its unique reproduction properties, gravure printing is primarily used for high-quality illustrative products, such as labels, packaging, and advertising catalogues. This specialization

makes gravure printing a focal point for researchers, especially in understanding the factors that influence the quality of printed images.

A detailed analysis of the basic principles of gravure printing is given in Szentgyörgyvölgyi (2016). In particular, special attention is paid to the transfer of ink at high speeds (in 1 – 3 ms), because, with the help of gravure printing, a much larger amount of ink can be transferred to the imprint than in most other printing technologies, thereby ensuring the reproduction of a wide range of tones.

Gladwell (1980) emphasizes that the ideal substrates for gravure printing are paper, cardboard, and film materials with a smooth surface (i.e., coated, supercalendered) since effective ink transfer depends on the full contact of the printing plate with the printing substrates. In Nandakumar and Paramasivam (2006), the authors note that gravure printing can reproduce images with a high screen ruling: 100, 120, 150, 175, 225, and 300 lines/cm. Printing using 175 lines/cm is popular.

As is known, the printing section of the gravure printing press consists of an ink supply system, a gravure and impression cylinder and a blade (Kipphan, 2001, p. 48). For high-speed printing presses, the best option is to use a closed ink system, thanks to which the evaporation of the solvent is reduced, in contrast to an open system, where there is no control of the evaporation of the solvent and the ink does not mix well. The closed system also uses ink viscosity control. In this system, every time the ink is returned from the ink fountain, it is filtered, and a solvent is added to maintain the desired viscosity of the ink. In addition to this closed ink application system, a spray system is also used for very high-speed printing presses, where an ink pump feeds ink to nozzles directed towards the cylinder. The surface of the nozzle always remains wet and never dries out. This system is also completely closed.

Gravure printing presses use several different designs of doctor blade, which is set at a certain angle (55 – 65 degrees) and removes the remaining ink from the non-image areas of the printing plate.

A steel printing cylinder is usually made with a hard rubber coating that can withstand high pressure. The rubber coating has a thickness of 12 to 20 mm. Its hardness ranges from 60 to 100 according to Shore A, depending on the type of the printing substrate. The amount of pressure in the printing zone (up to ~ 500 N/m^2) depends on the characteristics of the elasticity of the cylinder coating, the properties of the substrate, and the type of image being printed.

One of the challenges in ensuring the quality of imprints is the well-established balance of the interaction of the structural subsystems of the printing press, in particular plate cylinder and the inking and printing units with the substrate. It is known that the design of the impression cylinder significantly affects the deformation of its coating during printing. It was investigated that with constant deformation of the coating of the impression cylinder, the internal tension decreases and a relaxation phenomenon is observed, which leads to a gradual decrease in pressure in the printing area (Davies, et al., 2006). The larger the width of the printing press, the more pressure must be applied to obtain the desired width of the printing area. Significant pressure on the edges of a large-diameter cylinder causes deflection of the cylinder and resulting uneven distribution of pressure in the printing area. In such cases, there is a difference in image quality across the printing width and problems related to the passage of the reel substrate, which affects the quality of the printed image. Due to the high speed of gravure printing presses, ink transfer takes 1–3 ms. In this short time, the ink must be uniformly transferred from the small cells of the printing plate to the surface of the substrate (Davies, et al., 2006).

Therefore, it is relevant to study the behaviour of the the behavior of the printing substrate and printing plate elements system, to determine the factors affecting the stress–strain state of the contacting elements during the formation of an imprint in gravure printing presses.

The work reported here is aimed at studying the process of ink transfer from the gravure printing plate to the printing substrate using mathematical modelling to assist in ensuring the quality of the obtained imprints.

2. Objectives and methods of research

The objective of the research was to improve the process of obtaining imprints on a BOBST Lemanic 820 Riviera gravure printing press on cardboards with a grammage of 200 to 500 g/m^2 at a printing speed of v = 250 m/min. It was assumed that the plate cylinder should have the same diameter along the entire length, allowable micro-uniformity of 0.01 to 0.02 mm, a certain stiffness and maximum deflection within 0.05 to 0.1 mm.

The plate cylinder is made of steel, with a top coating of nickel, copper, and chrome. Thus, the tonal coverage of the image on the imprint from the lightest to the darkest areas is determined by different depths, as well as the distances between the screen cells. The

impression cylinder is covered with elastomer with a thickness of 30 to 40 mm. The thicker and more elastic the coating of the impression cylinder, the lower the pressure over the total contact surface during printing. When the cylinder coating thickness decreases, the required printing pressure increases.

The ratio of screen cells and the distances between them (cell walls) is an important parameter that affects the volume of the cell, the quality of imprints and the mechanical stability of the plate. The width of the cell wall affects the ability of the engraved surface to transfer ink. If the width of the cell wall between cells is large, then, when printing, a drop of ink must move across the width between cells when contacted with the substrate, which has no ink, to form a continuous image. The consequence of this failing to occur is results in unevenness of the image, on which it is then possible to see the screen structure.

The area occupied by screen lines is the absorption area of some part of the image itself. Accordingly, the wider the screen cell wall separation, the larger the area of the reproduced image is lost, and it is printed with certain defects. These defects, however, are almost invisible without special devices. This happens because the screen lines are so small in width (with a ratio of cells to cell separation greater than 1:2) that they cannot be noticed with the naked eye. The screen line carries a mechanical load. To provide it with the necessary mechanical stability, the minimum possible width of the inter-cell wall should be provided. Therefore, screens with a different width ratios of transparent and opaque elements in the range from 1:1 to 1:9 are used.

For the BOBST Lemanic 820 Riviera press considered in this study, the ratio of the width of print element and non-print element on the printing plate was 1:3. It should be noted that the researchers recommend creating wider lines on the printing plate (1:5; 1:6; 1:7; 1:8; 1:9) with increased printing speed to increase the durability of the plate.

It is known that for a square screen with a different ruling, but the same ratio of cell walls and cells, the area occupied by the cells in percentage terms, is the same, and the volume of the cells depends only on the depth of the cell and the angle of inclination of the edges of the cell. At higher printing press speeds and high pressure, the cylinder coating is severely damaged, heated and often cracked. Therefore, in many solutions to the problem in the printing press, the cylinder is cooled.

Mathematical modelling methods were used for theoretical research into the abovementioned phenomena.

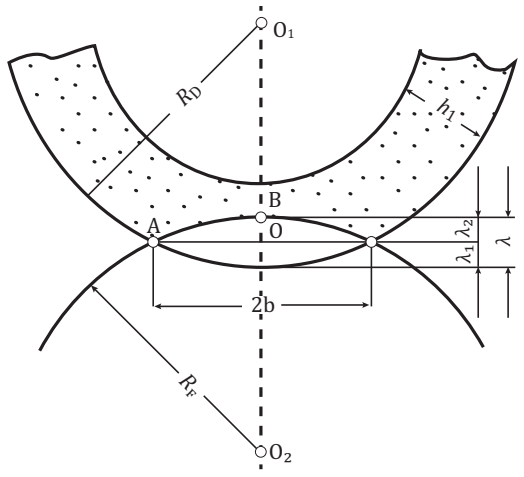

Figure 1: Scheme for calculating the pressure when printing by the gravure printing method where R_D is the radius of the impression cylinder, R_F is the radius of the plate cylinder and λ is the deformation

3. The proposed model and its discussion

Let us consider an example of calculating pressure when printing on a gravure printing press (Figure 1).

$$2b = \sqrt{\frac{2R_D R_F \lambda}{R_D + R_F}} \qquad [1]$$

According to Equation [1], for the radius of the plate cylinder R_F = 318 mm and the radius of the impression cylinder R_D = 180 mm, the width of the printing contact area 2b will be 15.2 mm at deformation (compression) of the coating λ = 0.5 mm and 21.4 mm at λ = 1.0 mm. The relative deformation, i.e. applied strain ε, of the cylinder coating during printing is determined by the Equation [2], where *h*1 is the coating thickness (see Figure 1):

$$\varepsilon = \frac{\lambda}{H} \qquad [2]$$

Hooke's purely elastic law does not work in practice between the stress of the load and its deformation (where the stress is directly proportional to the relative deformation of the material).

According to the equation of Tir (1965):

$$\sigma = (E\varepsilon)^{\frac{1}{m}} \qquad [3]$$

where σ is the stress, m is the power factor, which depends on the material properties, and E is the elastic modulus of the material. ε is the relative strain.

In the article (Raske, Hewson, Kapur and Boer, 2017), the authors provide a heterogeneous model for the formation of gravure imprints with discrete cells and partially consider the conditions of contact of the printed roll material with the printing plate. However, they focus their research on the relationship between the properties of inks and the shape of the coating layer. However, they do not detail the stress-strain state of the elements of the printing system. Studies (Tir, 1965) have shown that with constant deformation of the coating of a printing cylinder, the internal stress decreases and the relaxation phenomenon is observed, which leads to a gradual decrease in the pressure of the coating in the printing zone and stresses in it. The pressure concerning load relaxation is calculated using Maxwell's equation:

$$P = P_0 e^{\frac{-t}{T}} \quad [4]$$

where P is the printing pressure when the cylinder coating operates with a constant deformation, P_0 is the printing pressure when the coating operates with a variable deformation, e is the natural logarithm base, t is the duration of the printing pressure, T is the relaxation time corresponding to the time of change in the cylinder coating stress.

Depending on the pressure force in the printing area, the width of the contact strip between the printing plate and the coating of the impression cylinder ranges from 10 to 25 mm (Chubak and Uhryn, 2023). The larger the width of the printing press, the more external force must be applied to provide the necessary contact pressure to obtain the required width of the printing area. In practice, this force is often referred to as "pressure" because it is adjusted via a hydraulic pressure mechanism, but the resultant is nonetheless a force. However, due to the force being applied to the ends of the cylinder, significant pressure on the end edges of a large-diameter cylinder causes deflection of the cylinder and hence uneven distribution of pressure in the printing area. In such cases, there is a difference in image quality across the print width and problems related to the passage of the web (printing substrate), which affects the accuracy of both colour matching and image alignment.

Modern presses use pressure-compensated impression cylinders, which consist of a core with bearings and a rotating shell with a skin, where two independent sources of force significantly affect the deflection curve of the cylinder: one of them acts on both edges, the other on the trunnions. Axial pressure is transmitted to the rotating shell through bearings located in the middle of the impression cylinder. By changing the hydraulically generated forces, the necessary linear profiles of optimal pressure can be obtained to ensure consistent quality printing and correct, precise transport of the reel substrate through the printing and inking units of the printing press. There are well-known NIPCO cylinders that allow precise pressure to the plate cylinder to be set within the printing area over its entire width. Such cylinders consist of a fixed axis, on which a special steel cape covered with elastomer with a hardness of 80÷850 shore A is placed. The elastomeric coating makes it possible to ensure the same uniform pressure along the entire length of the printing area and ensure the proper quality of imprints.

The conducted morphological analysis of the structure of the printing and inking units of web-fed gravure printing presses confirmed the significant influence of their design on the distribution of pressure in the printing area and ensuring the appropriate quality of imprints (Chubak and Uhryn, 2023).

As previously mentioned, one of the main quality parameters is the full correspondence of the imprint to the original, including the geometric accuracy of image reproduction. One of the determining factors in this regard is the stress–strain state of the objects in direct contact during the printing process. The macro mechanics of the contact of cylindrical bodies, including those with an elastomeric or other nonlinearly elastic coating, have been studied quite fully, starting with the classic works of Hertz (1881; 1882), Boussinesq (1885) and Reynolds (1876) and mentioning several reviews of individual aspects of contact problems (Sulym, 2007; Kozachok, Martyniak and Slobodian, 2018; Sulym and Piskozub, 2004; Goryacheva, 1998; Martynyak and Serednytska, 2017; Ballarini, 1990; Gladwell, 1999; Johnson, 1985; Nemat-Nasser, 1999; Batra, Levinson and Betz, 1976; Bentall and Johnson, 1967).

However, macro mechanics of contact do not provide an opportunity to control the micro properties of contacting elements in the printing process, in particular raster elements, the size of which are orders of magnitude smaller than the size of the area of direct contact between the impression cylinder and the printing substrate. If there is a need for precision micro printing, it is necessary. Consider the micromechanics of contact.

The area of direct contact S is surrounded by a dashed frame in Figure 2. To consider the features of mechanical contact in the direct printing area, it is enough to consider the contact problem of two half-spaces with different mechanical properties, at the contact boundary of which there are inhomogeneities, the presence of which significantly disturbs the stress-deformed state in their vicinity (Figure 3) (Muskhelishvili, 1953; Sulym, 2007; Sulym and Piskozub, 2004; 2017; Gladwell, 1980; 1999; Johnson, 1985; Nemat-Nasser,

1999; Sulim and Piskozub, 2008; Boussinesq, 1885; Hertz, 1881; 1882).

We will consider the quasi-static contact of the half-space S_2 with the rigid S_1 base (Figure 3). We assume that the stress–strain state in the centre of the contact area for reasons of symmetry corresponds to the conditions of plane deformation. Shallow hole cells with a length of $2a$ and a height of $h(x)$ are located at the contact boundary of the base with the substrate with a regular spacing period $d\left(2a \gg h, 2a < d\right)$.

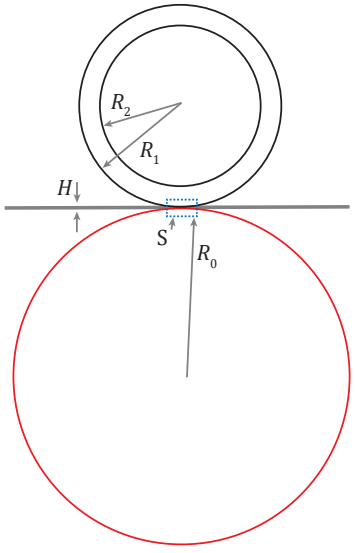

Figure 2: Model of contact of impression cylinders with the printing substrate in the gravure printing process (R_0- radius of the plate cylinder , R_1 and R_2 - radius of the impression cylinder with and without coating, H - thikness of printing substrate, S - zone of direct microcontact)

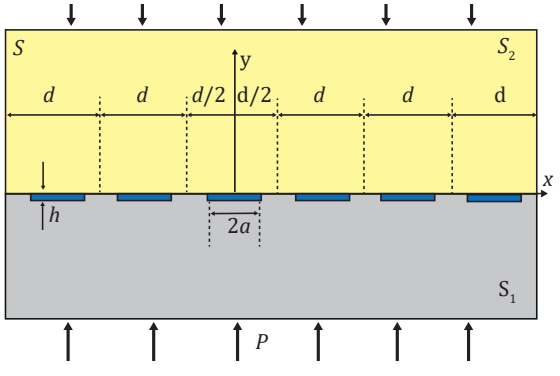

Figure 3: Micromechanical contact of raster cells with the substrate in the direct printing area (P – external pressure, 2a – cell width, h – cell depth, S – area of direct contact*)*

Boundary conditions in the areas of direct contact S_1 and S_2 expressed in spatial tensor components:

$$a \le \left|x - nd\right| \le \frac{d}{2}, \quad n = 0, \pm 1, \pm 2, \ldots \qquad [5]$$

$$\sigma_{xy}\left(x \pm 0\right) = 0, \quad u_y\left(x \pm 0\right) = 0$$

and in the areas of contact of the cell material with S_2:

$$\left|x - nd\right| < a, \quad n = 0, \pm 1, \pm 2, \ldots \qquad [6]$$

$$\sigma_{xy}\left(x \pm 0\right) = 0, \quad \sigma_{yy}\left(x \pm 0\right) = -P\left(x\right)$$

where $P(x)$ is the contact pressure caused by the presence of a liquid filler in the cells.

According to the methodology (Muskhelishvili, 1953; Sulym, 2007; Kozachok, Martyniak and Slobodian, 2018; Sulym and Piskozub, 2004; 2008; 2017; 2021; Piskozub, 2020; Pasternak and Sulym, 2011), the presence of thin inhomogeneities (cells) is modelled by an unknown jump of stresses and strains on their middle surface

$$\left(\sigma_{yy1}\left(\varsigma\right) - i\sigma_{xy1}\left(\varsigma\right)\right) - \left(\sigma_{yy2}\left(\varsigma\right) - i\sigma_{xy2}\left(\varsigma\right)\right) = \qquad [7]$$
$$f_1\left(\varsigma\right) - if_2\left(\varsigma\right),$$

$$\left(u'_{y1}\left(\varsigma\right) + iu'_{x1}\left(\varsigma\right)\right) - \left(u'_{y2}\left(\varsigma\right) + iu'_{y2}\left(\varsigma\right)\right) =$$
$$f_3\left(\varsigma\right) + if_4\left(\varsigma\right),$$

$$\varsigma = x + nd \quad \left(n = 0, \pm 1, \pm 2, \ldots\right)$$

Here σ_{yy1}, σ_{xy1} and σ_{yy2}, σ_{xy2} *denote the normal and tangential stresses in the contact zone of the half-spaces* S_1 *and* S_2, respectively. u'_{y1}, u'_{x1}, u'_{y2}, u'_{y2} denotes the respectively strains.

And due to boundary conditions (5), (6)

$$f_j\left(\varsigma\right) = f_j\left(x\right) \quad \left(j = 1, 2, 3, 4\right) \qquad [8]$$

$$f_j\left(\varsigma\right) = 0 \quad \left(j = 1, 2, 3, 4\right) \text{ at}$$

$$x \in \left[-d; d\right] \setminus \left[-a; a\right]$$

In addition, we have

$$f_j\left(\varsigma\right) = 0 \quad \left(j = 1, 2, 3\right) \text{ on the entire axis} \qquad [9]$$

$$Ox : x \in \left(-\infty; \infty\right)$$

Taking into account the periodicity of the problem, the field of stresses and displacements can be represented in the form of a superposition (Muskhelishvili, 1953; Kozachok, Martyniak and Slobodian, 2018;

Martynyak and Kryshtafovych, 2000; Martynyak and Serednytska, 2017):

$$\sigma_{yy}(z)-i\sigma_{xy}(z)=\sigma^0_{yy}(z)-i\sigma^0_{xy}(z)+ \sum_{n=-\infty}^{\infty}\left(\hat{\sigma}^{(n)}_{yy}(z)-i\hat{\sigma}^{(n)}_{xy}(z)\right), \quad z\in S \qquad [10]$$

$$u_y(z)+iu_x(z)=u^0_y(z)+iu^0_x(z)+ \sum_{n=\infty}^{\infty}\left(\hat{u}^{(n)}_y(z)+i\hat{u}^{(n)}_x(z)\right)$$

where $\sigma^0_{yy}(z),\sigma^0_{xy}(z),u^0_y(z),u^0_x(z)$ are components of the stress-strain state known from the homogeneous problem of contact of two half-spaces S_1 and S_2 without inhomogeneities in the contact area, and $\hat{\sigma}^{(n)}_{yy}(z),\hat{\sigma}^{(n)}_{xy}(z),\hat{u}^{(n)}_y(z),\hat{u}^{(n)}_x(z)$ are the unknown perturbations from jumps, $f_j(\varsigma)(j=1,2,3,4)$ caused by the presence of hole-cells.

The components of the stress tensor under plane deformation conditions can be expressed through a Airy function $U(x,y)$ (Muskhelishvili, 1953; Sulym, 2007; Kozachok, Martyniak and Slobodian, 2018)

$$\sigma_{xx}=\frac{\partial^2U}{\partial x^2},\ \sigma_{yy}=\frac{\partial^2U}{\partial y^2},\ \sigma_{xy}=-\frac{\partial^2U}{\partial x\partial y} \qquad [11]$$

which makes it possible to write the equilibrium equation in the form of a biharmonic equation

$$\Delta\Delta U=0 \qquad [12]$$

Using the well-known presentation of the biharmonic function through the Kolosov-Mushkelishvili complex potentials $\Phi(z),\Psi(z)$ (Muskhelishvili, 1953) and the methodology of works (Muskhelishvili, 1953; Sulym, 2007; Sulym and Piskozub, 2004; 2008; 2017; 2021; Piskozub, 2020; Martynyak and Kryshtafovych, 2000; Martynyak and Serednytska, 2017; Pasternak and Sulym, 2011) the components of the stress tensor and the displacement vector in each of considered S_k for a plane problem can be written using two complex potentials

$$\sigma_{yyk}-i\sigma_{xyk}=\Phi_k(z)+\overline{\Phi_k(z)}+ z\overline{\Phi'_k(z)}+\overline{\Psi_k(z)}, \qquad [13]$$

$$2G_k\left(u'_{xk}+iu'_{yk}\right)=\kappa_k\Phi_k(z)- \overline{\Phi_k(z)}-z\overline{\Phi'_k(z)}-\overline{\Psi_k(z)}$$

$$\left(z=x+iy\in S_k;\ \rightleftarrows\ \rightleftarrows\ k=1,2\right),$$

which are holomorphic in these half-planes and going to zero at infinity.

We define the functions $\Phi_1(z)$ in the upper half-plane and $\Phi_2(z)$ in the lower half-plane as follows (analytical continuation through unloaded sections) (Muskhelishvili, 1953; Sulym, 2007; Sulym and Piskozub, 2008):

$$\Phi_k(z)=-\overline{\Phi_k}(z)-z\overline{\Phi_k}(z)-\overline{\Psi_k}(z) \qquad [14]$$

$$\left(z\in S_j;k,l=1,2;l=3-k\right)$$

From here, replacing $z=x+iy$ with $\bar{z}=x-iy$, its complex conjugate, we get

$$\overline{\Psi_k(z)}=-\overline{\Phi_k(z)}-\Phi_k(\bar{z})-\overline{z\Phi'_k(z)} \qquad [15]$$

$$\left(z\in S_k;\ k=1,2\right)$$

Substituting this Equation [15] into Equation [13], and assuming that it is loaded by a field of uniform stresses at infinity $\sigma^\infty_{yy}=-P$, we get

$$\sigma_{yyk}(z)-i\sigma_{xyk}(z)= \Phi_k(z)-\Phi_k(\bar{z})+(z-\bar{z})\overline{\Phi'_k(z)}+\sigma^\infty_{yy},\quad (z\in S_k) \qquad [16]$$

$$2G_k\left[u'_{xk}(z)+u'_{yk}(z)\right]= \kappa_k\Phi_k(z)+\Phi_k(\bar{z})-(z-\bar{z})\overline{\Phi'_k(z)}-\frac{3-\kappa_k}{4}\sigma^\infty_{yy};$$

Here G_k – shear modules, ν_k – Poisson's coefficients, such that $\kappa_k = 3 - 4\nu_k$ – Mushelishvili's constants for plane deformation of half-space materials S_k. Passing in [16] to the limit at $z \to x$, taking into account the fact that $\lim_{z\to x}\left[(\bar{z}-\bar{z})\overline{\Phi'(z)}\right]=0$, and also that if z goes to the Ox axis from the lower (respectively, upper) half-plane S_k, then $\bar{z}$ goes to the same point on the Ox axis, only moving from the upper (lower) half-plane, we get

$$\sigma_{yyk}(x)-i\sigma_{xyk}(x)=\Phi^{\pm}_k(x)-\Phi^{\mp}_k(x),\quad k=\begin{Bmatrix}2\\1\end{Bmatrix} \qquad [17]$$

$$2G_k\left(u'_{xk}(x)+iu'_{yk}(x)\right)= \kappa_k\Phi^{\pm}_k(x)+\Phi^{\mp}_k(x),\qquad k=\begin{Bmatrix}2\\1\end{Bmatrix} \qquad [18]$$

Values in curly brackets mean that in equations [17], [18] and similar ones, the upper sign corresponds to the value $k = 2$; the lower one is $k = 1$. Applying the methodology of works [9-11, 21] can be obtained

$$\hat{\sigma}^{(n)}_{yy}(z)-i\hat{\sigma}^{(n)}_{xy}(z)= \Phi_k(z)-\Phi_k\left(\bar{z}+2nd\right)+ \left(z-\bar{z}-2nd\right)\overline{\Phi'_k(z)}, \qquad [19]$$

$$2G_k\left(\hat{u}^{(n)}_y(z)-i\hat{u}^{(n)}_x(z)\right)= \kappa_k\Phi_k(z)+\Phi_k\left(\bar{z}+2nd\right)- \left(z-\bar{z}-2nd\right)\overline{\Phi'_k(z)}\qquad z\in S$$

where

$$\Phi_k(z) = -\frac{(-1)^{3-k}}{\pi\Upsilon}\sum_{n=-\infty}^{\infty}\int_{-a+nd}^{a+nd}\frac{f_4(t)}{t-z}\mathrm{d}t \qquad [20]$$

$$z \in \mathrm{S}_k\,(k=1,2),$$

$$\Upsilon = \frac{1+\kappa_1}{2G_1} + \frac{1+\kappa_2}{2G_2}$$

Using the summation equation

$$\sum_{n=-\infty}^{\infty}\frac{1}{z-nd} = \frac{\pi}{d}\mathrm{ctg}\left(\frac{\pi z}{d}\right) \qquad [21]$$

we will rewrite the potentials [19] in the form

$$\Phi_k(z) = \frac{(-1)^{3-k}}{d\Upsilon}\int_{-a}^{a} f_4(t)\mathrm{ctg}\frac{(t-z)}{d}\mathrm{d}t, \qquad [22]$$

$$z \in S_k\,(k=1,2)$$

Then the contact pressure defined by Equation [6] can be calculated using the Equation [23]

$$P(x) = -\sigma_{yy}(x,\pm 0) \qquad [23]$$

$$= -\frac{2}{d\Upsilon}\int_{-a}^{a} f_4(t)\mathrm{ctg}\frac{\pi(t-z)}{d}\mathrm{d}t - \sigma_{yy}^{\infty}$$

from which it is easy to obtain the singular integral equation with the Hilbert kernel to determine the unknown jump $f_4(x)$

$$\frac{2}{d}\int_{-a}^{a} f_4(t)\,\mathrm{ctg}\,\frac{\pi(t-z)}{d}dt = \Upsilon\left(P - P(x)\right) \qquad [24]$$

To solve Equation [24], it is convenient to use the substitution of variables

$$\xi = \mathrm{tg}\left(\frac{\pi x}{d}\right),\ \eta = \mathrm{tg}\left(\frac{\pi t}{d}\right), \qquad [25]$$

$$\alpha = \mathrm{tg}\left(\frac{\pi a}{d}\right),\quad \beta = \mathrm{tg}\left(\frac{\pi b}{d}\right)$$

Then Equation [24] transforms into a Equation [25] with a Cauchy-type kernel

$$\int_{-\alpha}^{\alpha}\frac{f_4(\eta)}{\eta-\xi}d\eta = F(\eta) = \qquad [26]$$

$$\frac{\Upsilon d}{2\left(1+\xi^2\right)}\left(P - P(\xi)\right),$$

$$|\xi| \le \alpha$$

which has a solution

$$f_4(\xi) = \frac{1}{\pi^2\sqrt{\alpha^2-\xi^2}} \qquad [27]$$

$$\left\{-\int_{-\alpha}^{\alpha}\frac{\sqrt{\alpha^2-\eta^2}\,F(\eta)}{\eta-\xi}\mathrm{d}\eta + \int_{-\alpha}^{\alpha} f_4(\xi)\mathrm{d}\xi\right\}$$

Taking into account that at the ends of the cells $\hat{u}_y^{(n)}(x \pm na) = -h\ \ (n = 0, \pm 1, \pm 2, \ldots)$, we have an additional condition

$$\int_{-\alpha}^{\alpha} f_4(\xi)\mathrm{d}\xi = 0 \qquad [28]$$

The pressure $P(\xi)$ can be found using the equation of state of a compressible barotropic fluid (Muskhelishvili, 1953; Sulym, 2007; Kozachok, Martyniak and Slobodian, 2018)

$$V_h e^{\frac{P_h}{B}} = V_0 \qquad [29]$$

where $V_0 = 2ah$ is the initial volume of a rectangular cell in profile, V_h is the volume of liquid per unit cell length in the transverse direction, and B is modulus of volume elasticity of liquid.

From Equation [27] taking into account Equation [26], we get the solution

$$f_4(\xi) = \frac{\Upsilon d\left(P - P_h\right)\xi\sqrt{\alpha^2+1}}{2\pi\left(1+\xi^2\right)\sqrt{\alpha^2-\xi^2}},\quad |\xi| \le \alpha \qquad [30]$$

Integrating Equation [30], we get increase in cell volume

$$\Delta u_y(\xi) = \int_{-\alpha}^{\xi} f_4(\xi)d\xi = \qquad [31]$$

$$-\frac{\Upsilon d\left(P - P_h\right)}{2\pi}\mathrm{arcth}\left(\frac{\sqrt{\alpha^2-\xi^2}}{\sqrt{\alpha^2+1}}\right) +$$

$$h,\quad |\xi| \le \alpha$$

Then the contact pressure of the surfaces can be calculated from the equation

$$P(x) = \qquad [32]$$

$$\frac{\left|\mathrm{tg}\left(\frac{\pi x}{d}\right)\right|\sqrt{\mathrm{tg}^2\left(\frac{\pi a}{d}\right)+1}}{\sqrt{\mathrm{tg}^2\left(\frac{\pi x}{d}\right)-\mathrm{tg}^2\left(\frac{\pi a}{d}\right)}}\left(P - P_h\right) + P_h,$$

$$a \le |x - kd| \le \frac{d}{2}$$

Equation [29] for determining the fluid pressure P_h after applying the substitution of variables [27] and taking into account

$$V_0 = \frac{dh}{\pi}\int_{-\alpha}^{\alpha}\frac{d\xi}{1+\xi^2} = \frac{2hd\cdot\mathrm{arctg}(\alpha)}{\pi} \qquad [33]$$

takes the form

$$e^{\frac{P_h}{B}\left(-\frac{\Upsilon d\left(P-P_h\right)}{4}\right)} \qquad [34]$$
$$\left(\ln\left(\alpha^2+1\right)+2h\cdot\operatorname{arctg}\left(\alpha\right)\right)-2h\cdot\operatorname{arctg}\left(\alpha\right)=0$$

This equation does not have an analytical solution, so it should be solved by numerical methods. It is worth noting that the less compressible the liquid is, the less the contact pressure changes over the entire contact surface, including the intervals of direct contact of the half-spaces. The direction in [34] of the modulus of volume elasticity of the liquid to infinity (incompressible fluid, $B \to \infty$) leads to the result that the pressure of an incompressible fluid is equal to the applied load $P(x) = P$ and therefore, the pressure over the entire surface of the body is also constant and equal to the applied load. That is, there is no effect of the presence of hole cells as perturbations of the stress-strain state in the contact area.

With the help of the method, it is possible to carry out several numerical calculations for various parameters of changing the size and location of the cells on the printing plate, as well as changes in the mechanical properties of materials of half-spaces and fluids under external load in the range $0 < P < P^{\infty}$, where

$$P^{\infty} = \Upsilon B \ln\left(\left(\frac{\operatorname{arctg}\left(\alpha\right)}{\left(\frac{\pi\ln\left(\alpha^2+1\right)}{\ln\left(\sqrt{\alpha^2+1}+\alpha\right)}+4\operatorname{arctg}\left(\alpha\right)\right)^{-1}}\right)+ \frac{2\pi h}{d\ln\left(\sqrt{\alpha^2+1}+\alpha\right)}\right) \qquad [35]$$

i.e. the load at which the contact of the border of the half-space S_2 with the base of the cells at depth $y = -h$.

4. Conclusions

Thus, taking into account the theoretical principles of macro- and micromechanics of the contact of system elements in the gravure printing process, it is possible to control their properties. Using the method of mathematical modelling, it is possible to calculate and control the load in the contact area of the printing substrate and printing plate with ink-filled printing elements, ensuring the quality of imprints on various materials, taking into account their structure and thickness.

References

Anon., 2006. Trends in digital engraving. *Flexo & Gravure International*, 2, pp. 20–24.

Ballarini, R., 1990. A rigid line inclusion at a bimaterial interface. *Engineering Fracture Mechanics*, 37(1), pp. 1–5. https://doi.org/10.1016/0013-7944(90)90326-c.

Batra, R.C., Levinson, M. and Betz, E., 1976. Rubber covered rolls – the thermoviscoelastic problem. A finite element solution. *International Journal for Numerical Methods in Engineering*, 10 (4), pp. 767–785. https://doi.org/10.1002/nme.1620100405.

Bentall, R. H. and Johnson, K. L., 1967. Slip in the rolling contact of two dissimilar elastic rollers. *International Journal of Mechanical Sciences*, 9(6), pp. 389–404. https://doi.org/10.1016/0020-7403(67)90043-4.

Boussinesq, J., 1885. *Application des potentiels à l'étude de l'équilibre et du mouvement des solides élastiques*. Paris: Gauthier-Villars.

Chubak, Y. and Uhryn, Y., 2023. Morphological analysis of problems of the imprints quality related to the structure of printing and inking systems of gravure printing presses. *Printing and Publishing*, 2(86), pp. 91–101.

Davies, G.R. and Claypole, T. C., 2006. Effect of viscosity on ink transfer in gravure printing. In: *Proceedings of the 33rd International Research conference of Iarigai*, Leipzig, Germany, pp. 235–244.

Drago, A. and Pindera, M., 2007. Micro-macromechanical analysis of heterogeneous materials: Macroscopically homogeneous vs periodic microstructures. *Composites Science and Technology*, 67(6), pp. 1243–1263. https://doi.org/10.1016/j.compscitech.2006.02.031.

Gladwell, G.M., 1999. On inclusions at a bi-material elastic interface. *Journal of Elasticity*, 54(1), pp. 27–41.

Gladwell, G.M.L., 1980. *Contact problems in the classical theory of elasticity.* Dordrecht: Springer Netherlands.

Goryacheva, I.G., 1998. *Contact mechanics in tribology*. Dordrecht: Springer Netherlands. https://doi.org/10.1007/978-94-015-9048-8.

Hertz, H., 1881. Über die Berührung fester elastischer Körper. *Journal für die reine und angewandte Mathematik*, 92, pp. 156–171.

Hertz, H., 1882. Über die Berührung fester elastischer Körper und über die Harte. *Verhandlungen des Vereins zur Beförderung des Gewerbfleißes*, 1882, pp. 449–463.

Johnson, K.L., 1985. *Contact Mechanics*. Cambridge: Cambridge University Press.

Kipphan, H., 2001. *Handbook of Print Media: Technologies and Production Methods.* Berlin: Springer. ISBN 978-3540673262.

Kozachok, O., Martynyak, R., and Slobodian, B., 2018. *Vzaemodiia til z rehuliarnoho reliiefu za naiavnosti mizhkontaktnoho seredovyshcha*. Lviv, Ukraine: Rastr-7 (in English: *Interaction Between Bodies with Regular Relief in the Presence of an Interstitial Medium*).

Martynyak, R. and Kryshtafovych, A., 2000. Friction contact of two elastic half-planes with local recesses in boundary. *Journal of Friction and Wear*, 21(4), pp. 6–15.

Serednytska, K. and Martynyak, R., 2017. *Контактні задачі термопружності для міжфазних тріщин в біматеріальних тілах.* (in English: *Contact problems of thermoelasticity for interface cracks in bimaterials*).

Muskhelishvili, N. I., 1953. *Some basic problems of the mathematical theory of elasticity: Fundamental equations, plane theory of elasticity, torsion and bending. Groningen*: Noordhoff.

Nandakumar, M. and Paramasivam, A., 2006. *Gravure, flexo and screen printing*. Sivakasi: Arasan Ganesan Polytechnic College.

Nemat-Nasser, S. and Hori, M., 1999. *Micromechanics: Overall Properties of Heterogeneous Materials*. 2nd rev. ed. Cambridge: Cambridge University Press.

Pasternak, Y.M. and Sulym, G.T., 2011. Models of Fine Inhomogeneities Considering the Possibility of Their Non-Ideal Contact with the Environment. *Dnipro University Bulletin: Mechanics Series*, 15(5), pp. 200–210.

Piskozub, Y. Z. and Sulym, H. T., 2021. Modeling of deformation of the bimaterial with thin Non-linear interface inclusion. *Researches in Mathematics and Mechanics*, 2(36), pp. 40–57. https://doi.org/10.18524/2519-206x.2020.2(36).233748.

Piskozub, Y.Z., 2020. Effect of surface tension on the antiplane deformation of bimaterial with a thin interface microinclusion. Mathematical Modeling and Computing, 8(1), pp. 69–77. https://doi.org/10.23939/mmc2021.01.069.

Raske, N., Hewson, R., Kapur, N. and Boer, G., 2017. A predictive model for discrete cell gravure roll coating. *Physics of Fluids*, 29(6), 062101. https://doi.org/10.1063/1.4984127.

Reynolds, O., 1876. On rolling friction. *Philosophical Transactions of the Royal Society of London*, 166, pp. 155–175.

Stefanyshena, O. B. and Zorenko, O.V., 2020. Modern trends in the development of gravure printing. Technology and Technique of Typography, 3(69), pp. 34–42. https://doi.org/10.20535/2077-7264.3(69).2020.224199.

Sulim, G. T. and Piskozub, J. Z., 2008. Thermoelastic equilibrium of piecewise homogeneous solids with thin inclusions. *Journal of Engineering Mathematics*, 61, pp. 315–337. https://doi.org/10.1007/s10665-008-9225-3.

Sulym, G. and Piskozub, Y., 2004. Conditions of contact interaction of bodies: an overview. *Mathematical Methods and Physical and Mechanical fields*, 47(3), pp. 110–125.

Sulym, G. and Piskozub, Y., 2017. Nonlinear deformation of a thin interfacial inclusion. *Physical and Chemical Mechanics of Materials*, 53(5), pp. 24–30.

Sulym, G.T., 2007. *Fundamentals of the mathematical theory of thermoelastic equilibrium of deformable solids with thin inclusions*. Lviv: Research and Publishing Center of the National Academy of Sciences.

Szentgyörgyvölgyi, R., 2016. Gravure printing. In: J. Izdebska, S. Thomas, eds., eds. 1st ed. *Printing on Polymers*. Waltham: William Andrew. pp. 199–215. https://doi.org/10.1016/B978-0-323-37468-2.00012-9.

Tir, K.V., 1965. *Mechanics of printing machines*. Moscow.